Letter

Electronic correlations in the normal state of the kagome superconductor KV_3Sb_5

Jianzhou Zhao [1,2,*] Weikang Wu [2,3] Yilin Wang [4,†] and Shengyuan A. Yang [2]

[1]*Co-Innovation Center for New Energetic Materials, Southwest University of Science and Technology, Mianyang 621010, China*
[2]*Research Laboratory for Quantum Materials, Singapore University of Technology and Design, Singapore 487372, Singapore*
[3]*Division of Physics and Applied Physics, School of Physical and Mathematical Sciences, Nanyang Technological University, Singapore 637371, Singapore*
[4]*Hefei National Laboratory for Physical Sciences at Microscale, University of Science and Technology of China, Hefei, Anhui 230026, China*

(Received 28 March 2021; revised 30 May 2021; accepted 16 June 2021; published 28 June 2021)

Recently, intensive studies have revealed fascinating physics, such as charge density wave and superconducting states, in the newly synthesized kagome-lattice materials AV_3Sb_5 (A = K, Rb, Cs). Despite the rapid progress, fundamental aspects such as the magnetic properties and electronic correlations in these materials have not been clearly understood yet. Here, based on density functional theory plus single-site dynamical mean-field theory calculations, we investigate the correlated electronic structure and magnetic properties of the KV_3Sb_5 family materials in the normal state. We show that these materials are good metals with weak local correlations. The obtained Pauli-like paramagnetism and the absence of local moments are consistent with a recent experiment. We reveal that the band crossings around the Fermi level form three groups of nodal lines protected by the spacetime inversion symmetry, each carrying a quantized π Berry phase. Our result suggests that the local correlation strength in these materials appears to be too weak to generate unconventional superconductivity, and nonlocal electronic correlation might be crucial in this kagome system.

DOI: 10.1103/PhysRevB.103.L241117

The kagome lattice has attracted great interest in condensed matter physics research. As a prototype lattice with strong geometric frustration, the kagome lattice has been extensively studied in quantum magnetism [1,2] and was proposed as the host for a quantum spin-liquid state [3–6]. Itinerant electrons on a kagome lattice can realize a special band structure with Dirac cones and a flat band [7,8]. Further incorporating electron interaction effects, a rich variety of exotic effects have been predicted on the kagome lattice, such as charge bond order [9,10], spin or charge density waves (SDWs or CDWs) [11,12], charge fractionalization [13], a topological insulating state [14,15], and superconductivity [16,17]. Driven by these predictions, real materials that contain a kagome lattice have been actively explored [8,18–24].

Recently, a novel family of kagome materials AV_3Sb_5 (A = K, Rb, Cs) were synthesized [25]. These materials share the same layered structure, which contains active layers of a V kagome lattice. All the three compounds exhibit superconductivity at low temperature, with $T_c = 0.93$, 0.92, and 2.5 K, for KV_3Sb_5 [26], RbV_3Sb_5 [27], and CsV_3Sb_5 [28], respectively. Besides superconductivity, a CDW instability was observed at $T^* \sim 80$–100 K [25–32]. Interestingly, in the normal state above the CDW transition, these materials were revealed to be $\mathbb{Z}_2$ topological metals [28]. An angle-resolved photoemission spectroscopy (ARPES) experiment reported multiple Dirac points near the Fermi level. This is also supported by the Shubnikov–de Haas oscillation result that indicates highly dispersive low-energy bands with a rather low effective mass [27]. It was speculated that the Dirac electrons could play an important role in the observed large nonspontaneous anomalous Hall response [33,34].

Despite the rapid progress, there are still many puzzles on these materials to be addressed. For instance, a recent susceptibility measurement and muon spin relaxation and rotation (μSR) measurement both indicate the absence of local magnetic moments [35], which differs from the expectation from simple valence counting and appears to be in conflict with the observed extremely large anomalous Hall response [33,34]. Meanwhile, the nature of the superconductivity in these materials is still under debate [27,30,32,34,36–42]. Some recent theoretical and experimental works suggested that the superconductivity and CDW might be unconventional [30,34,38–40,43,44], which hints at important electron correlation effects. However, an understanding of the correlation strength in these materials is still lacking.

In this Letter, we investigate the correlated electronic structure and magnetic properties of KV_3Sb_5, using a combination of density functional theory (DFT) and dynamical mean-field theory (DMFT) calculations [45,46]. By considering the on-site Coulomb interaction, we show that the KV_3Sb_5 family materials are weakly correlated metals in the normal state. Our obtained temperature independence of Pauli-like magnetic susceptibility behavior is consistent with experimental results [26,35], confirming the absence of local moments. From an atomic configuration analysis and a calculated hybridization function, we attribute this result to the strong p-d hybridization that leads to the delocalization of V d electrons. The low-energy bands are only weakly affected by the on-site

*jzzhao@swust.edu.cn
†yilinwang@ustc.edu.cn

interaction. We analyze the linear band crossings near the Fermi level, and show that they are actually not isolated Dirac points, instead belonging to three groups of nodal lines in the Brillouin zone (BZ), protected by the spacetime inversion symmetry in the absence of spin-orbit coupling (SOC). One group (three rings) is centered around the M point, and the other two vertically traverse the BZ. Our result indicates that the local electron-electron correlation alone is not sufficient to account for unconventional superconductivity (if it indeed exists); nonlocal correlations might be required for such an effect. This also echoes recent works on the CDW state of these materials, which suggest that nonlocal correlations play an important role in its formation [30].

Method. We perform fully charge self-consistent DFT+DMFT calculations using the EDMFTF package [47], based on the full-potential linear augmented plane-wave method implemented in the WIEN2K code [48,49]. The k-point mesh for the Brillouin zone integration is $17 \times 17 \times 10$, and the plane-wave cutoff $K_{\max}$ is given by $R_{\mathrm{MT}} \times K_{\max} = 8.0$. We employed the generalized gradient approximation (GGA) with the Perdew-Burke-Ernzerhof (PBE) realization [50] as the exchange-correlation functional. The atomic spheres R_{MT} are 2.50, 2.50, and 2.65 a.u. for K, V, and Sb, respectively. We use projectors with an energy window from -10 to 10 eV relative to the Fermi level to construct V $3d$ local orbitals. A rotationally invariant form of a local on-site Coulomb interaction Hamiltonian parametrized by Hubbard U and Hund's coupling J_H is applied on all five V $3d$ orbitals. We choose $U = 5.0$ eV and $J_H = 0.7$ eV in this Letter, which are typical values used previously for $SrVO_3$ [51,52], V_2O_3 [53,54], and VO_2 [55]. Considering that KV_3Sb_5 should have weaker correlations than the oxides, these values serve as the upper bounds for studying correlation effects. Smaller values of U and J_H are also tested and result in weaker correlation effects [56], as expected. The impurity problem is solved by the hybridization expansion version of the continuous-time quantum Monte Carlo (CTQMC) solver [57]. We choose an "exact" double-counting scheme developed by Haule [58], in which the Coulomb repulsion in real space is screened by a combination of Yukawa and dielectric functions. The self-energy on the real frequency is obtained by the analytical continuation method of maximum entropy [47]. The effective mass enhancement by correlations is defined by $m^*/m_{\mathrm{DFT}} = 1/\mathcal{Z}$, where $\mathcal{Z}$ is the quasiparticle weight. To avoid a large error bar in the analytic continuation, we directly obtain $\mathcal{Z} = 1 - \frac{\partial\, \mathrm{Im}\, \Sigma(i\omega_n)}{\partial \omega_n}|_{\omega_n \to 0^+}$ from the polynomial fit to self-energies on the first ten Matsubara frequencies. We have tested that SOC has negligible effects on the low-energy band structure, so it is omitted in the calculation.

Lattice structure. The crystal structure for KV_3Sb_5 is shown in Fig. 1. The material has a layered structure, with the $P6/mmm$ space group. The most important motif is the kagome lattice formed by the V atoms. The kagome plane is sandwiched between two layers of Sb_1 atoms, each consisting of a honeycomb lattice. Within the same lattice plane, the Sb_2 atoms fill the large voids of the kagome lattice. The low-energy states are dominated by these three atomic layers, which form a V-Sb slab. The alkali atoms fill the region between the V-Sb slabs, and they mainly play the role of electron donors. It follows that the three materials in the family should exhibit very similar electronic properties, which is confirmed by experiments and also by our calculation. Hence, we will mainly focus on KV_3Sb_5 in the following discussion.

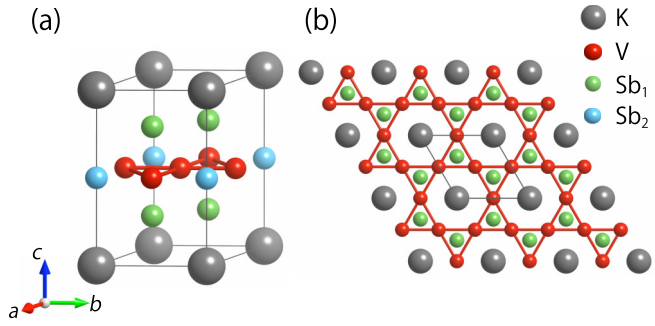

FIG. 1. (a) Crystal structure of KV_3Sb_5. Here, a unit cell is shown. (b) Top view of KV_3Sb_5. The red lines show the kagome lattice of V. Sb atoms in the V plane are labeled as Sb_2. Other Sb atoms are labeled as Sb_1.

We adopt the experimental lattice parameters in the calculation [25]. The values are given in the Supplemental Material (SM) [56].

Orbital occupancy and mass enhancement. Let us first consider the occupation n_d of V $3d$ orbitals in KV_3Sb_5. From our DFT+DMFT calculations, the $3d$ occupancy of vanadium is about 3.169. The orbital-resolved occupancy number ranges from 0.526 to 0.785 with $d_{x^2-y^2}$ (d_{xy}) as the least (most) occupied orbitals. These numbers are listed in Table I. The results for the other two members are quite similar, with $n_d = 3.112$ for RbV_3Sb_5 and 3.206 for CsV_3Sb_5.

Then we consider the mass enhancement $m^*/m_{\mathrm{DFT}} = 1/\mathcal{Z}$, which is widely used to characterize the strength of electronic correlations. This ratio is unity for an uncorrelated normal metal, and is much larger than unity for a strongly correlated system (e.g., $m^*/m_{\mathrm{DFT}} \approx 7$ in the iron-based superconductor FeTe [59,60]). Our calculation results for KV_3Sb_5 are listed in Table I. One observes that the mass enhancement of the V $3d$ electrons is quite weak, ranging from 1.284 ($d_{x^2-y^2}$) to 1.442 (d_{xz}). The other two members RbV_3Sb_5 and CsV_3Sb_5 have similar values. This indicates that the KV_3Sb_5 family materials are weakly correlated metals in their normal states. Our DFT+DMFT results are consistent with the experimental

TABLE I. The orbital-resolved V $3d$ occupation n_d and effective mass enhancement m^*/m_{DFT} for KV_3Sb_5, RbV_3Sb_5, and CsV_3Sb_5 obtained from DFT+DMFT calculation at $T = 300$ K. The V $3d$ occupations obtained by DFT, n_d^{DFT}, are also presented for reference.

		d_{z^2}	$d_{x^2-y^2}$	d_{xz}	d_{yz}	d_{xy}
KV_3Sb_5	$n_d^{\mathrm{DFT}} = 3.302$	0.735	0.527	0.561	0.555	0.925
	$n_d = 3.169$	0.678	0.526	0.605	0.575	0.785
	m^*/m_{DFT}	1.354	1.284	1.442	1.308	1.340
RbV_3Sb_5	$n_d^{\mathrm{DFT}} = 3.312$	0.732	0.524	0.562	0.558	0.936
	$n_d = 3.112$	0.683	0.540	0.614	0.484	0.791
	m^*/m_{DFT}	1.356	1.282	1.445	1.308	1.342
CsV_3Sb_5	$n_d^{\mathrm{DFT}} = 3.252$	0.726	0.513	0.560	0.571	0.882
	$n_d = 3.206$	0.686	0.532	0.606	0.591	0.791
	m^*/m_{DFT}	1.351	1.292	1.446	1.313	1.347

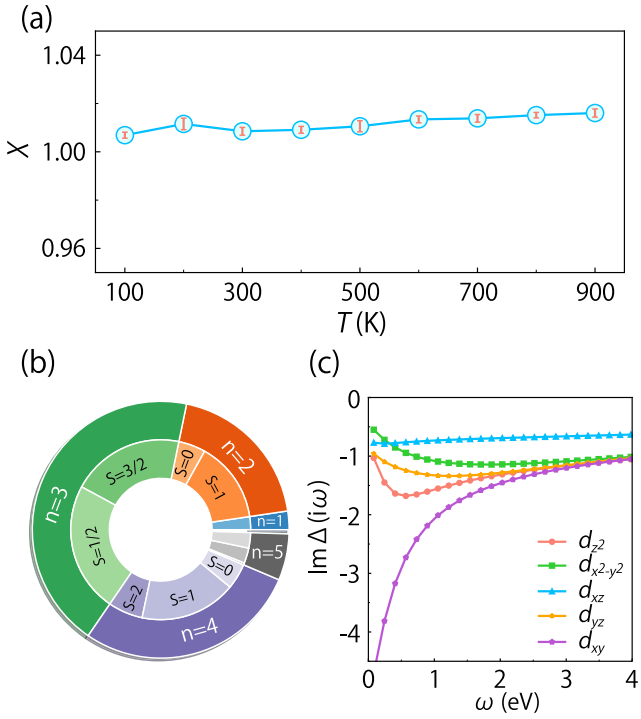

FIG. 2. (a) The calculated spin susceptibility χ as a function of temperature T. The error bar indicates the fluctuation of the results for the last five charge self-consistent iterations. (b) The valence histograms of the V $3d$ shell obtained by CTQMC. (c) Imaginary part of the hybridization function on Matsubara frequencies at $T = 300$ K.

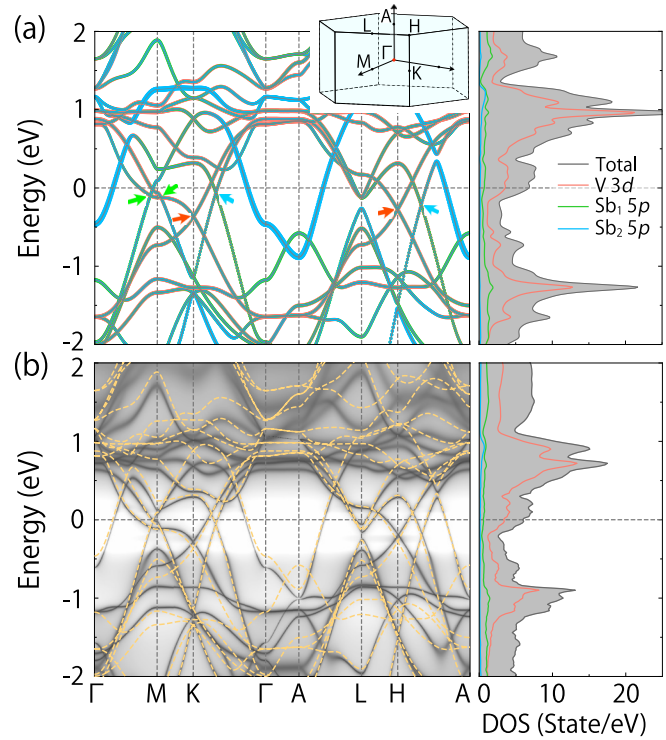

FIG. 3. (a) DFT band structure and DOS of KV_3Sb_5. The weight of V $3d$, Sb_1, and Sb_2 $5p$ orbitals are indicated by red, green, and blue colors, respectively. (b) k-resolved spectral function obtained by DFT+DMFT at $T = 300$ K. The DFT band structure is plotted with gold dashed lines for reference.

observation of low effective mass and highly dispersive bands in KV_3Sb_5 [33] and RbV_3Sb_5 [27].

Spin susceptibility. To investigate the magnetic properties, we calculate the static local spin susceptibility, defined as

$$\chi = \int_0^\beta \langle S_z(\tau) S_z(0) \rangle d\tau, \tag{1}$$

by the CTQMC approach. Here, $\beta = 1/(k_B T)$, and τ is the imaginary time. The calculation is done for the normal state in the temperature range from 100 to 900 K. The obtained χ vs T result is presented in Fig. 2(a). Clearly, the susceptibility exhibits a paramagnetism with an almost flat line independent of T in the normal state. For good metals, this behavior indicates the dominance of a Pauli paramagnetic response from itinerant electrons and the absence of local moments (local moments instead would give a T dependence typically following the Curie-Weiss law). Indeed, the Pauli susceptibility estimated from the density of states (DOS) at the Fermi level is about $1.482 g^2 \mu_B^2$/eV, which agrees well with the value $\sim 1.008 g^2 \mu_B^2$/eV obtained from the CTQMC calculation at 300 K. Here, g is the g-factor and μ_B is the Bohr magneton. Our result agrees well with the recent magnetic measurements on KV_3Sb_5 [26,35].

To further shed light on this result, in Fig. 2(b), we present the probability distribution for the different atomic configurations for the V $3d$ shell. The DMFT atomic basis is constructed from the five d orbitals with the size of $\sum_n C_{10}^n = 848$ for seven different occupancies with $n = 0, 1, \ldots, 6$. One finds that the $n = 3$ state has the highest probability with 43.7%, followed by $n = 4$ with 28.2%, and $n = 2$ with 19.4%. Within the dominant $n = 3$ state, the probability for the low-spin state is 23.4%, slightly higher than that for the high-spin state $S = 3/2$ (∼20.3%). Note that in the atomic limit, the configuration with occupancy $n_d = 3$ should typically favor the high-spin state according to the Hund's rule. Here, the close competition between different occupancy and spin states indicates a strong charge and spin fluctuation in the normal state of KV_3Sb_5. This can be attributed to the strong hybridization between V $3d$ and Sb $5p$ orbitals. In Fig. 2(c), we plot the hybridization functions for the V $3d$ orbitals, which indicate a substantial delocalization of these orbitals (all having imaginary parts larger than 0.5 eV), especially for the d_{xy} orbital.

Correlated electronic structure. The DFT band structure and DOS are shown in Fig. 3(a). One observes that the bands within 2 eV around the Fermi level are dominated by the V $3d$ and Sb $5p$ states. There is a large peak in DOS around 1 eV with a V $3d$ character, which could be attributed to the flat band featured by the kagome network. There are several linear band crossings around the Fermi level. The band with a V $3d$ character exhibits a van Hove singularity at the M point around -63 meV. Meanwhile, a highly dispersive band with Sb_2 $5p$ character forms two large electron pockets at the Γ and A points.

As a comparison, the correlated electronic spectral function from our DFT+DMFT calculation is shown in Fig. 3(b). One can see that the low-energy bands are not significantly

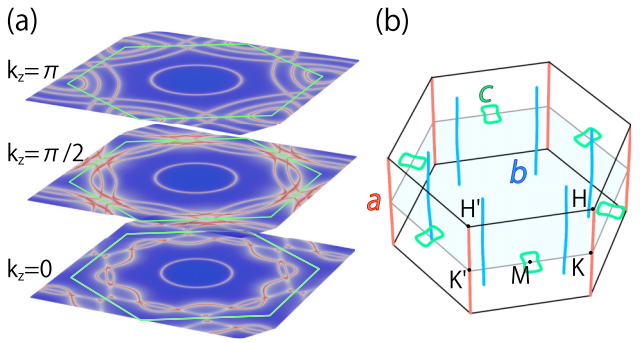

FIG. 4. (a) Fermi-surface plot for $k_z = 0$, $k_z = \pi/2$, and $k_z = \pi$ planes by DFT+DMFT at $T = 300$ K. The BZ boundary is shown in green lines. (b) Three types of nodal lines a (red), b (blue), and c (green) in the BZ. Points on these lines are indicated with colored arrows in Fig. 3(a).

affected by the electronic correlations (the DFT bands are plotted with gold dashed lines in this figure for reference). The bands with V $3d$ characters between -1 and 1 eV are only slightly pushed above by the renormalization effect introduced by the correlation. The quasiparticle spectrum maintains a good coherence, indicating a negligible imaginary part of self-energy and a long quasiparticle lifetime. Overall, our result shows that KV_3Sb_5 is a weakly correlated metal.

In Fig. 4(a), we plot the DFT+DMFT Fermi surface contours in the $k_z = 0$, $\pi/2$, and π slices of the BZ. The most obvious feature is a highly two-dimensional (2D) electron pocket at the center of the BZ, which has been observed in a previous ARPES experiment on CsV_3Sb_5 [28]. According to our calculation [56], this 2D electron pocket is contributed mainly by the p_z orbitals on Sb_2 atoms. A Fermi surface with a hexagonal petal shape is located close to the BZ boundary in the $k_z = 0$ plane, which is mainly from the V $3d_{xy}$ states. Six round pockets with a V $3d_{xz/yz}$ character appear close to the K and K' points.

Topological nodal lines. The linear band crossings observed in Fig. 3(a) around the Fermi level were previously interpreted as Dirac points and as a feature of the kagome lattice [26,28]. Nevertheless, we note the following two points. First, the system preserved both inversion $\mathcal{P}$ and time-reversal $\mathcal{T}$ symmetries. Under the combined $\mathcal{PT}$ symmetry, an isolated (twofold) Dirac point cannot exist in a 3D system [61]. Second, the Dirac points for the standard kagome model appear at the high-symmetry K and K' points. However, in Fig. 3(a), linear crossings also appear at other locations, such as Γ-M, K-Γ, and H-A paths.

We focus on the crossings indicated by the arrows in Fig. 3(a) and scan the BZ to trace the nodal structure. We find that these points are in fact located on three groups of nodal lines, as depicted in Fig. 4(b). Group a contains two nodal lines pinned along the K-H and K'-H' paths; group b contains six nodal lines constrained in the three vertical mirror planes; and group c has three members lying in the horizontal mirror plane, each forming a ring around the M point. Here, each of the nodal lines carries a topological charge given by the quantized π Berry phase $\nu = \oint_C \mathrm{Tr}\,\boldsymbol{\mathcal{A}} \cdot d\boldsymbol{k} \mod 2\pi$, where C is a closed path encircling the line, $\boldsymbol{\mathcal{A}}$ is the Berry connection for the occupied bands, and the π quantization is enforced by the $\mathcal{PT}$ symmetry in the absence of SOC. Perturbations that respect the $\mathcal{PT}$ symmetry may deform the shapes of the nodal lines but cannot destroy them. Including SOC can open a small gap ($\sim$20 meV) at these nodal lines.

Discussion. Our DFT+DMFT study indicates that KV_3Sb_5 family materials are good metals with weak electronic correlation effects. The mass enhancement is only around 1.3–1.4. The obtained Pauli-like paramagnetism and absence of a local moment are consistent with recent experimental results. The revealed nodal line structures could be probed by ARPES. Due to the π Berry phase of the nodal lines, we expect a suppressed backscattering for the in-plane transport, which is an important factor underlying the materials' good conductivity.

The origin of the large anomalous Hall response in these materials is still an open problem. We note that the kagome lattice usually has strong magnetic fluctuations. This is evidenced by the competing energies of different magnetic configurations, estimated from a simple DFT+U calculation [56]. The magnetic fluctuations might play a role in the anomalous Hall response and other properties.

It should be noted that our current study can only deal with on-site correlations. Nonlocal correlations are not included. Our result hence implies that local correlations alone are not sufficient for realizing an unconventional superconductivity. If the superconductivity is indeed unconventional, it would hint at an important role played by nonlocal correlations, such as in the example of $Ba_{0.51}K_{0.49}BiO_3$ [62]. In SM Sec. IV [56], we compare the band structures obtained by DMFT and the hybrid functional approach, which implies sizable nonlocal exchange effects in KV_3Sb_5.

The authors thank G. Xu, Z.-G. Chen, M. R. Kim, and D. L. Deng for valuable discussions. This work was supported by the National Natural Science Foundation of China (No. 11604273), and the Singapore Ministry of Education AcRF Tier 2 (MOE2019-T2-1-001). Y. Wang was supported by USTC Research Funds of the Double First-Class Initiative (No. YD2340002005). The computational work was performed on resources of the Texas Advanced Computing Center and National Supercomputing Centre, Singapore.

[1] F. Pollmann, P. Fulde, and K. Shtengel, Phys. Rev. Lett. **100**, 136404 (2008).
[2] M. P. Shores, E. A. Nytko, B. M. Bartlett, and D. G. Nocera, J. Am. Chem. Soc. **127**, 13462 (2005).
[3] S. Yan, D. A. Huse, and S. R. White, Science **332**, 1173 (2011).
[4] T.-H. Han, J. S. Helton, S. Chu, D. G. Nocera, J. A. Rodriguez-Rivera, C. Broholm, and Y. S. Lee, Nature (London) **492**, 406 (2012).

[5] T. Han, S. Chu, and Y. S. Lee, Phys. Rev. Lett. **108**, 157202 (2012).

[6] M. Fu, T. Imai, T.-H. Han, and Y. S. Lee, Science **350**, 655 (2015).

[7] N. J. Ghimire and I. I. Mazin, Nat. Mater. **19**, 137 (2020).

[8] L. Ye, M. Kang, J. Liu, F. von Cube, C. R. Wicker, T. Suzuki, C. Jozwiak, A. Bostwick, E. Rotenberg, D. C. Bell, L. Fu, R. Comin, and J. G. Checkelsky, Nature (London) **555**, 638 (2018).

[9] A. O'Brien, F. Pollmann, and P. Fulde, Phys. Rev. B **81**, 235115 (2010).

[10] F. Pollmann, K. Roychowdhury, C. Hotta, and K. Penc, Phys. Rev. B **90**, 035118 (2014).

[11] S.-L. Yu and J.-X. Li, Phys. Rev. B **85**, 144402 (2012).

[12] W.-S. Wang, Z.-Z. Li, Y.-Y. Xiang, and Q.-H. Wang, Phys. Rev. B **87**, 115135 (2013).

[13] A. Rüegg and G. A. Fiete, Phys. Rev. B **83**, 165118 (2011).

[14] H.-M. Guo and M. Franz, Phys. Rev. B **80**, 113102 (2009).

[15] J. Wen, A. Rüegg, C.-C. J. Wang, and G. A. Fiete, Phys. Rev. B **82**, 075125 (2010).

[16] M. L. Kiesel and R. Thomale, Phys. Rev. B **86**, 121105(R) (2012).

[17] M. L. Kiesel, C. Platt, and R. Thomale, Phys. Rev. Lett. **110**, 126405 (2013).

[18] Q. Wang, S. Sun, X. Zhang, F. Pang, and H. Lei, Phys. Rev. B **94**, 075135 (2016).

[19] E. Liu, Y. Sun, N. Kumar, L. Muechler, A. Sun, L. Jiao, S.-Y. Yang, D. Liu, A. Liang, Q. Xu, J. Kroder, V. Süß, H. Borrmann, C. Shekhar, Z. Wang, C. Xi, W. Wang, W. Schnelle, S. Wirth, Y. Chen *et al.*, Nat. Phys. **14**, 1125 (2018).

[20] J.-X. Yin, S. S. Zhang, H. Li, K. Jiang, G. Chang, B. Zhang, B. Lian, C. Xiang, I. Belopolski, H. Zheng, T. A. Cochran, S.-Y. Xu, G. Bian, K. Liu, T.-R. Chang, H. Lin, Z.-Y. Lu, Z. Wang, S. Jia, W. Wang, and M. Z. Hasan, Nature (London) **562**, 91 (2018).

[21] J.-X. Yin, S. S. Zhang, G. Chang, Q. Wang, S. S. Tsirkin, Z. Guguchia, B. Lian, H. Zhou, K. Jiang, I. Belopolski, N. Shumiya, D. Multer, M. Litskevich, T. A. Cochran, H. Lin, Z. Wang, T. Neupert, S. Jia, H. Lei, and M. Z. Hasan, Nat. Phys. **15**, 443 (2019).

[22] Q. Wang, Y. Xu, R. Lou, Z. Liu, M. Li, Y. Huang, D. Shen, H. Weng, S. Wang, and H. Lei, Nat. Commun. **9**, 1 8 (2018).

[23] Y. Xu, J. Zhao, C. Yi, Q. Wang, Q. Yin, Y. Wang, X. Hu, L. Wang, E. Liu, G. Xu, L. Lu, A. A. Soluyanov, H. Lei, Y. Shi, J. Luo, and Z.-G. Chen, Nat. Commun. **11**, 3985 (2020).

[24] J.-X. Yin, W. Ma, T. A. Cochran, X. Xu, S. S. Zhang, H.-J. Tien, N. Shumiya, G. Cheng, K. Jiang, B. Lian, Z. Song, G. Chang, I. Belopolski, D. Multer, M. Litskevich, Z.-J. Cheng, X. P. Yang, B. Swidler, H. Zhou, H. Lin *et al.*, Nature (London) **583**, 533 (2020).

[25] B. R. Ortiz, L. C. Gomes, J. R. Morey, M. Winiarski, M. Bordelon, J. S. Mangum, I. W. H. Oswald, J. A. Rodriguez-Rivera, J. R. Neilson, S. D. Wilson, E. Ertekin, T. M. McQueen, and E. S. Toberer, Phys. Rev. Materials **3**, 094407 (2019).

[26] B. R. Ortiz, P. M. Sarte, E. M. Kenney, M. J. Graf, S. M. L. Teicher, R. Seshadri, and S. D. Wilson, Phys. Rev. Materials **5**, 034801 (2021).

[27] Q. Yin, Z. Tu, C. Gong, Y. Fu, S. Yan, and H. Lei, Chin. Phys. Lett. **38**, 037403 (2021).

[28] B. R. Ortiz, S. M. L. Teicher, Y. Hu, J. L. Zuo, P. M. Sarte, E. C. Schueller, A. M. M. Abeykoon, M. J. Krogstad, S. Rosenkranz, R. Osborn, R. Seshadri, L. Balents, J. He, and S. D. Wilson, Phys. Rev. Lett. **125**, 247002 (2020).

[29] Y.-X. Jiang, J.-X. Yin, M. M. Denner, N. Shumiya, B. R. Ortiz, G. Xu, Z. Guguchia, J. He, M. S. Hossain, X. Liu, J. Ruff, L. Kautzsch, S. S. Zhang, G. Chang, I. Belopolski, Q. Zhang, T. A. Cochran, D. Multer, M. Litskevich, Z.-J. Cheng *et al.*, Nat. Mater. (2021), doi: 10.1038/s41563-021-01034-y.

[30] H. X. Li, T. T. Zhang, Y. Y. Pai, C. Marvinney, A. Said, T. Yilmaz, Q. Yin, C. Gong, Z. Tu, E. Vescovo, R. G. Moore, S. Murakami, H. C. Lei, H. N. Lee, B. Lawrie, and H. Miao, arXiv:2103.09769.

[31] Z. Liang, X. Hou, W. Ma, F. Zhang, P. Wu, Z. Zhang, F. Yu, J. J. Ying, K. Jiang, L. Shan, Z. Wang, and X. H. Chen, arXiv:2103.04760.

[32] H. Tan, Y. Liu, Z. Wang, and B. Yan, arXiv:2103.06325.

[33] S.-Y. Yang, Y. Wang, B. R. Ortiz, D. Liu, J. Gayles, E. Derunova, R. Gonzalez-Hernandez, L. Šmejkal, Y. Chen, S. S. P. Parkin, S. D. Wilson, E. S. Toberer, T. McQueen, and M. N. Ali, Sci. Adv. **6**, eabb6003 (2020).

[34] F. H. Yu, T. Wu, Z. Y. Wang, B. Lei, W. Z. Zhuo, J. J. Ying, and X. H. Chen, arXiv:2102.10987.

[35] E. M. Kenney, B. R. Ortiz, C. Wang, S. D. Wilson, and M. J. Graf, J. Phys.: Condens. Matter **33**, 235801 (2021).

[36] W. Duan, Z. Nie, S. Luo, F. Yu, B. R. Ortiz, L. Yin, H. Su, F. Du, A. Wang, Y. Chen, X. Lu, J. Ying, S. D. Wilson, X. Chen, Y. Song, and H. Yuan, arXiv:2103.11796.

[37] Z. Zhang, Z. Chen, Y. Zhou, Y. Yuan, S. Wang, J. Wang, H. Yang, C. An, L. Zhang, X. Zhu, Y. Zhou, X. Chen, J. Zhou, and Z. Yang, Phys. Rev. B **103**, 224513 (2021).

[38] C. C. Zhao, L. S. Wang, W. Xia, Q. W. Yin, J. M. Ni, Y. Y. Huang, C. P. Tu, Z. C. Tao, Z. J. Tu, C. S. Gong, H. C. Lei, Y. F. Guo, X. F. Yang, and S. Y. Li, arXiv:2102.08356.

[39] K. Y. Chen, N. N. Wang, Q. W. Yin, Y. H. Gu, K. Jiang, Z. J. Tu, C. S. Gong, Y. Uwatoko, J. P. Sun, H. C. Lei, J. P. Hu, and J.-G. Cheng, Phys. Rev. Lett. **126**, 247001 (2021).

[40] H. Chen, H. Yang, B. Hu, Z. Zhao, J. Yuan, Y. Xing, G. Qian, Z. Huang, G. Li, Y. Ye, Q. Yin, C. Gong, Z. Tu, H. Lei, S. Ma, H. Zhang, S. Ni, H. Tan, C. Shen, X. Dong, B. Yan, Z. Wang, and H.-J. Gao, arXiv:2103.09188.

[41] X. Chen, X. Zhan, X. Wang, J. Deng, X.-b. Liu, X. Chen, J.-g. Guo, and X. Chen, Chin. Phys. Lett. **38**, 057402 (2021).

[42] F. Du, S. Luo, B. R. Ortiz, Y. Chen, W. Duan, D. Zhang, X. Lu, S. D. Wilson, Y. Song, and H. Yuan, Phys. Rev. B **103**, L220504 (2021).

[43] Y. Wang, S. Yang, P. K. Sivakumar, B. R. Ortiz, S. M. L. Teicher, H. Wu, A. K. Srivastava, C. Garg, D. Liu, S. S. P. Parkin, E. S. Toberer, T. McQueen, S. D. Wilson, and M. N. Ali, arXiv:2012.05898.

[44] X. Wu, T. Schwemmer, T. Müller, A. Consiglio, G. Sangiovanni, D. D. Sante, Y. Iqbal, W. Hanke, A. P. Schnyder, M. M. Denner, M. H. Fischer, T. Neupert, and R. Thomale, arXiv:2104.05671.

[45] A. Georges, W. Krauth, and M. J. Rozenberg, Rev. Mod. Phys. **68**, 13 (1996).

[46] G. Kotliar, S. Y. Savrasov, K. Haule, V. S. Oudovenko, O. Parcollet, and C. A. Marianetti, Rev. Mod. Phys. **78**, 865 (2006).

[47] K. Haule, C.-H. Yee, and K. Kim, Phys. Rev. B **81**, 195107 (2010).

[48] P. Blaha, K. Schwarz, G. K. H. Madsen, D. Kvasnicka, J. Luitz, R. Laskowski, F. Tran, and L. D. Marks, *WIEN2k, An Augmented Plane Wave + Local Orbitals Program for Calculating Crystal Properties* (Karlheinz Schwarz, Techn. Universität Wien, Austria, 2018).

[49] P. Blaha, K. Schwarz, F. Tran, R. Laskowski, G. K. H. Madsen, and L. D. Marks, J. Chem. Phys. **152**, 074101 (2020).

[50] J. P. Perdew, K. Burke, and M. Ernzerhof, Phys. Rev. Lett. **77**, 3865 (1996).

[51] E. Pavarini, S. Biermann, A. Poteryaev, A. I. Lichtenstein, A. Georges, and O. K. Andersen, Phys. Rev. Lett. **92**, 176403 (2004).

[52] C. Taranto, M. Kaltak, N. Parragh, G. Sangiovanni, G. Kresse, A. Toschi, and K. Held, Phys. Rev. B **88**, 165119 (2013).

[53] K. Held, G. Keller, V. Eyert, D. Vollhardt, and V. I. Anisimov, Phys. Rev. Lett. **86**, 5345 (2001).

[54] K. Held, I. A. Nekrasov, G. Keller, V. Eyert, N. Blümer, A. K. McMahan, R. T. Scalettar, T. Pruschke, V. I. Anisimov, and D. Vollhardt, Phys. Status Solidi **243**, 2599 (2006).

[55] M. S. Laad, L. Craco, and E. Muller-Hartmann, Phys. Rev. B **73**, 195120 (2006).

[56] See Supplemental Material at http://link.aps.org/supplemental/10.1103/PhysRevB.103.L241117 for structural data, Fermi surface, DFT+U, and hybrid functional calculations, as well as the mass enhancement results with small Hubbard U, which includes Refs. [63–69].

[57] E. Gull, A. J. Millis, A. I. Lichtenstein, A. N. Rubtsov, M. Troyer, and P. Werner, Rev. Mod. Phys. **83**, 349 (2011).

[58] K. Haule, Phys. Rev. Lett. **115**, 196403 (2015).

[59] Z. P. Yin, K. Haule, and G. Kotliar, Nat. Mater. **10**, 932 (2011).

[60] A. Tamai, A. Y. Ganin, E. Rozbicki, J. Bacsa, W. Meevasana, P. D. C. King, M. Caffio, R. Schaub, S. Margadonna, K. Prassides, M. J. Rosseinsky, and F. Baumberger, Phys. Rev. Lett. **104**, 097002 (2010).

[61] H. Weng, Y. Liang, Q. Xu, R. Yu, Z. Fang, X. Dai, and Y. Kawazoe, Phys. Rev. B **92**, 045108 (2015).

[62] C. H. P. Wen, H. C. Xu, Q. Yao, R. Peng, X. H. Niu, Q. Y. Chen, Z. T. Liu, D. W. Shen, Q. Song, X. Lou, Y. F. Fang, X. S. Liu, Y. H. Song, Y. J. Jiao, T. F. Duan, H. H. Wen, P. Dudin, G. Kotliar, Z. P. Yin, and D. L. Feng, Phys. Rev. Lett. **121**, 117002 (2018).

[63] A. I. Liechtenstein, V. I. Anisimov, and J. Zaanen, Phys. Rev. B **52**, R5467(R) (1995).

[64] J. Heyd, G. E. Scuseria, and M. Ernzerhof, J. Chem. Phys. **118**, 8207 (2003).

[65] A. V. Krukau, O. A. Vydrov, A. F. Izmaylov, and G. E. Scuseria, J. Chem. Phys. **125**, 224106 (2006).

[66] G. Kresse and J. Furthmüller, Phys. Rev. B **54**, 11169 (1996).

[67] G. Kresse and J. Furthmüller, Comput. Mater. Sci. **6**, 15 50 (1996).

[68] P. E. Blöchl, Phys. Rev. B **50**, 17953 (1994).

[69] P. E. Blöchl, C. J. Först, and J. Schimpl, Bull. Mater. Sci. **26**, 33 (2003).